Interfacial Friction Factor Model for Two-dimensional Film Flow

Jin-Hwa Yang [a], Hyoung-Kyu Cho [a*], Dong-Jin Euh [b], Goon-Cherl Park [a]
[a] *Nuclear Thermal-Hydraulic Eng. Lab., Seoul Nat. Univ., Gwanak 599, Gwanak-ro, Gwanak-gu, Seoul 151-742*
[b] *Korea Atomic Energy Research Ins., 989-111, Daedeok-daero, Yuseong-gu, Daejeon 305-600*
[*] *Corresponding author: chohk@snu.ac.kr*

1. Introduction

Safety analysis codes such as RELAP-5, CATHARE3, TRACE, MARS and SPACE developed multi-dimensional modules to simulate multi-dimensional phenomena in the nuclear reactor more appropriately. However, since experimental studies and modellings as to multi-dimensional phenomena are incomplete, the multi-dimensional modules have used one-dimensional models and correlations to reproduce the multi-dimensional phenomena. Using the one-dimensional models and correlations for multi-dimensional problems has limitations due to the compatibility. In this study, experimental study of upper downcomer two-phase flow which is also the multi-dimensional problem will be described and two-dimensional interfacial friction factor model will be also suggested.

The upper downcomer two-phase flow of a nuclear reactor is one of important multi-dimensional problems. In particular, in a Direct Vessel Injection (DVI) system of Advanced Power Reactor 1400 (APR 1400), the Emergency Core Coolant (ECC) is injected onto the upper downcomer from 2.1 m higher position than one of cold-leg. The injected ECC interacts with the lateral steam flow from the nuclear reactor core during the reflood phase in the Large Break Loss of Coolant accident (LBLOCA). The interaction between the falling film and lateral steam flow induces a two-phase multi-dimensional film flow. The amount of reflood coolant was determined by the effect of the interfacial drag between two fluids.

It can be dealt as annular flow or film flow regime in the aforementioned safety analysis codes. They have used interfacial drag coefficient model which was developed by one-dimensional experimental results. Wallis [1] model is a representative one to deal the interfacial friction factor with void fraction (or film thickness). It was developed with experimental data of annular flow from a vertical pipe. Fore [2] indicated that Wallis' model overestimates interfacial friction factor in thinner liquid film region and underestimates that in thicker liquid film region. Asali [3] suggested interfacial drag model with a dimensionless film thickness considering a roll wave effect. These models have been incorporated in multi-dimensional module of safety analysis codes and the verification and validation (V&V) have also been carried out recently.

However, it has some challenges because there are not sufficient local measurement experimental data to be used for validation benchmarks of the multi-dimensional modules. Thus, it is necessary to investigate the local measurement studies on a multi-dimensional film flow. The final purposes of this study are to develop an interfacial friction factor model according to the film flow with lateral air injection and to produce experimental data for validation of multi-dimensional thermal-hydraulic codes. In this paper, an experimental study simulating the upper downcomer will be presented. A rectangular shape 1/10 scaled down test facility was devised and measurements of local liquid film velocity and thickness were carried out. After that, the momentum conservation equations were set up with local measurement data and the interfacial friction factors according to two-dimensional film flow were produced.

2. Two-dimensional Film Flow Experiments

In this section, the 1/10 scaled-down experimental test facility, test conditions, local experimental methods to measure film velocity and thickness are described.

2.1 Description of Experimental Facility

A local experimental facility was designed to simulate the two-dimensional film flow, as shown in Fig. 1. It consists of an air supply system to provide lateral air flow and a water supply system to simulate the falling liquid film. In order to try the local measurement by Particle Image Velocimetry (PIV), an unfolded parallel acrylic plate was built rather than annulus shape one. The interfacial momentum exchange between two phases was investigated in the acrylic test section.

Water with fluorescent particles for PIV was injected through a 1-inch nozzle from storage tank by pump. The injected water impinged on the test section wall (1.4 m × 0.62 m × 0.025 m (W×H×D)) and made a liquid film running down on the flat plate wall. After that, the water returned to the storage tank through the drain line at the bottom of the test section.

Air was chosen as a gas phase fluid instead of steam to separate the condensation or heat transfer effect from the hydraulic effect. The air was injected by a blower along the 15.24 cm (6-inch) pipe. The air was uniformly distributed by a perforated plate in the expansion section. After an interaction between the injected air and falling

water, it was divided by a separator at the end of the test section.

2.2 Experimental Conditions

The test section was devised as 1/10 scale of APR 1400. The modified linear scaling method, which was developed by Yun [4], was adopted. It used a scaled down velocity that was divided by the square root of the scaling ratio. Under real conditions, it is assumed that the ECC might be injected at about a 2 m/s water velocity through the DVI line, and the velocity of lateral steam which comes from reactor core varied from 15 m/s to 45 m/s. Following the modified linear scaling, the 0.63 m/s of inlet liquid velocity and range of 5 to 15 m/s of transverse air velocity were recommended as experimental conditions. In this study, the 5 and 7 m/s of lateral air velocity was selected to determine the feasibility of the experimental methods for local measurements. As shown in Fig. 2, the control volume was maintained at up to a 7 m/s lateral air velocity, and the entrainment effect was also negligible. The experiment without an air injection was also considered as a reference case.

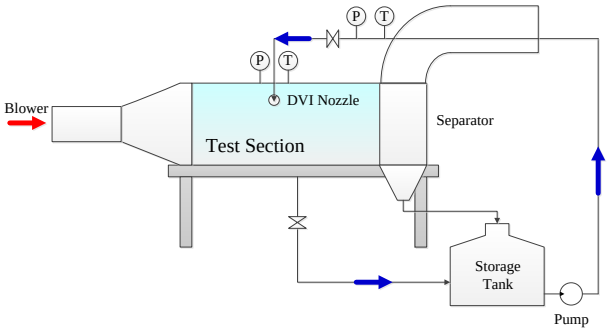

Fig. 1. Schematics of Experimental Facility

Table I: Test matrix for liquid film experiments

	Velocity(m/s)		
Inlet water velocity	0.63		
Lateral air velocity	0	5	7

(a) 0 m/s (b) 5 m/s (c) 7 m/s

Fig. 2. Control Volume for Measurements

2.3 Liquid Film Velocity Measurement

To measure the local liquid film velocity, the PIV is a desirable method. There are two types of PIV methods following the shape of the incident laser: sheet-PIV and volume-PIV. The sheet-PIV is used to measure the liquid velocity of a representative sheet face in a liquid flow. The incident laser should not be disturbed by the geometry of the test section or reflected by the free surface of the liquid. In addition, the transmitted area of the incident laser has to be maintained in spite of the laser attenuation effect.

In the case of a measurement of the liquid film velocity, there are two limitations to apply the sheet-PIV method. One is that the thickness of the liquid film flow is too narrow for a laser sheet to be transmitted. The other is that reflection on the film oscillation boundary and attenuation effect of the laser cannot retain enough light intensity.

To measure the liquid film velocity, we applied another PIV method: volume-PIV. It yielded the averaged velocity data along the depth direction. As shown in Fig. 3, two lasers lightened the fluorescent particles in the liquid film in front of the test section. This was suitable to maintain the light intensity since it is not disturbed by the film oscillation boundary or attenuation. The averaged velocity along the depth direction should be validated, and will be dealt with through an uncertainty analysis later.

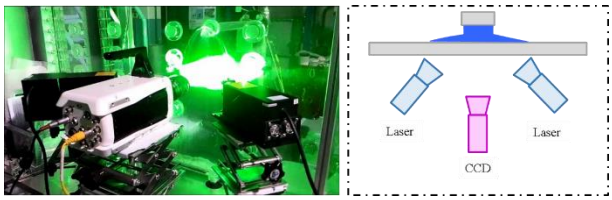

Fig. 3. Volume-PIV Method for Measurement of Liquid Film Velocity

The volume-PIV method produced the local velocity data of falling liquid film with a lateral air flow using the 1 to 20 μm fluorescent particles. The control volume was divided into 12 sub-grids to satisfy the field of view of a high-speed camera (Fig. 2). Each grid was a 50 mm × 35 mm (W×H) cell. The field of view was defined by the size of the fluorescent particles for the PIV. 1000 pictures of each grid were taken. The resolution of the pictures was 1280 × 960 pixels.

The liquid film oscillation was intensified by the lateral air injection, and the laser exposed the interface between the liquid and air, as shown in Fig. 4 (a). To overcome the image reflection problem, the 560 nm long-pass filter was used to eliminate the vestige of the interface (Fig. 4 (b)). The filtered images were analyzed by in-house PIV software, which was developed with the cross-correlation algorithm and the median filter (Kim [5]). After the cross correlation, 24 × 19 vectors were generated on each grid.

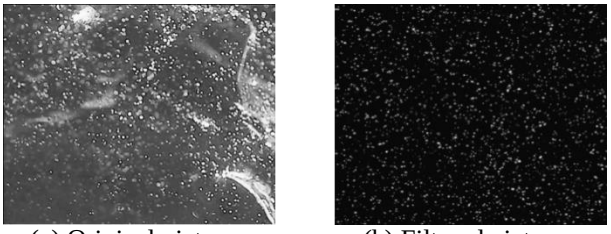

(a) Original picture (b) Filtered picture

Fig. 4. Effect of Long-pass Filter

2.3 Liquid Film Thickness Measurement

The ultrasonic thickness gauge is a widely accepted method to measure the thickness of the material. The pulse-echo type ultrasonic thickness gauge used the round-trip time of an ultrasonic wave, which reflects the boundary echo layer following Eq. (1).

$$\delta_f = \frac{c_f(\mathrm{T})\Delta t}{2} \quad (1)$$

where δ_f is the liquid film thickness, c_f is the sound speed in water, T is the temperature of water, and Δt is the round trip time of an ultrasonic wave. Fig. 5 shows the measuring points on the test section.

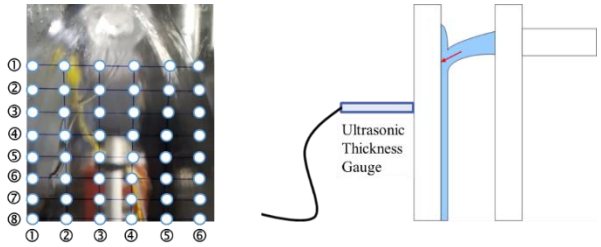

Fig. 5. Ultrasonic Thickness Gauge for Liquid Film Thickness Measurement

3. Experimental Results and Uncertainty Analysis

3.1 Liquid Film Velocity

The interaction between the falling liquid film and the lateral air induces momentum transfer through their interface. Fig. 6 shows the liquid film velocity vectors according to the increase of lateral air velocity. Fig. 6 (a) shows that the faster the lateral air injected, the larger the liquid film vector that appeared. On the contrary, Fig. 6 (b) indicates that the faster the lateral air was injected, the smaller liquid film vectors appeared. If the lateral air velocity increases, the relative velocity between the two fluids also increases. On the right side of the spreading liquid film width, the x-directional velocity vector has a negative value. The lateral air acted as a counter-current flow on the interface. Therefore, it made the x-directional velocity vector of the liquid film decrease. On the left side of the spreading liquid film width, the x-directional velocity vector has a positive value and the lateral air acted as a co-current flow on the interface. It consequently increased the x-directional velocity vector of liquid film. As a result, the relative velocity on the interface affects the velocity variation of the liquid film.

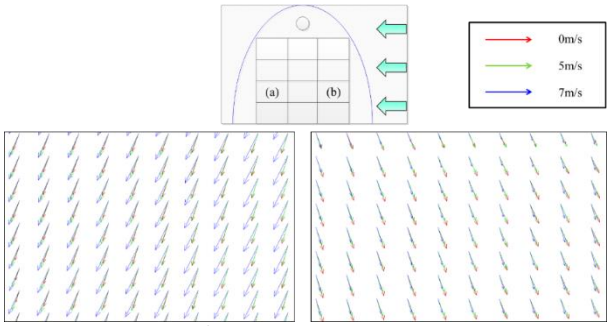

(a) Vectors on left side (b) Vectors on right side

Fig. 6. Momentum Exchange according to Lateral Air Velocity Increase

Assembling the vectors of each grid yielded vector fields on the control volume, as shown in Fig. 7. These show that the vector distribution and streamlines vary along the lateral air velocity increase. Without the lateral air injection (0 m/s), the velocities of liquid film are almost symmetric along the centerline of the inlet nozzle (x = 0 mm). With the lateral air injection (5 and 7 m/s), the velocities are varied according to the aforementioned trends.

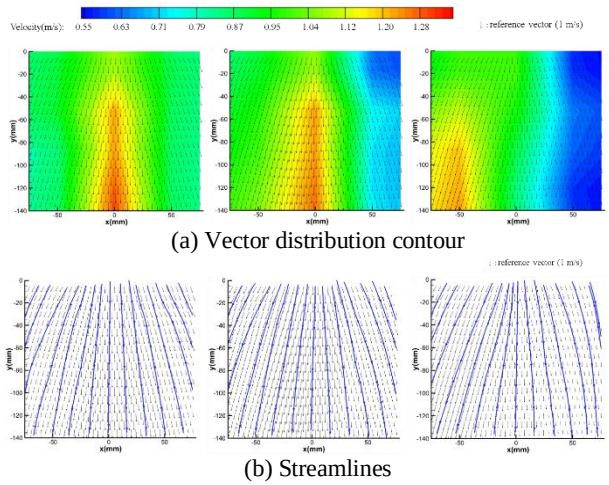

(a) Vector distribution contour

(b) Streamlines

Fig. 7. Vector Distribution and Streamlines with Different Lateral Air Velocity

3.2 Liquid Film Thickness

The liquid film thickness is one of the important parameters of a two-dimensional liquid film flow since it contains void fraction information. In addition, it has been dealt with as a significant correlation factor to product the empirical models of interfacial friction factor. Fig. 8 shows the liquid film thickness variation on the horizontal centerline (red solid line) of the control volume according to different air velocities. The aforementioned trend of liquid film velocity indicated that the amount of the momentum exchange increased as the lateral air velocity grew. In the case of liquid film thickness, a similar trend was confirmed. Comparisons

among the peak point values of the three cases showed a 17 to 56 % increase of thickness.

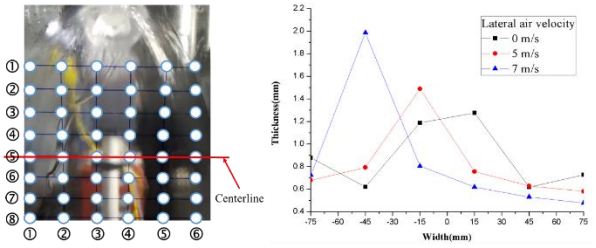

Fig. 8. Movement of Peak Thickness as Lateral Air Velocity Increases

3.3 Local Measurement Results

Fig. 9 shows the results of two-dimensional liquid film velocity and thickness according to the difference of lateral air velocity. The velocity vector and thickness distribution seems to be symmetric without a lateral air injection, as shown in Fig. 7 (a). However, it is noted that when the lateral air was injected, the velocity vectors and thickness distributions of liquid film were biased to the left side (Fig. 7 (b) and (c)). If the momentum transfer effects can be quantified through the local measurement experiments, a model for the interfacial friction factor can be developed and be used to validate the multidimensional code.

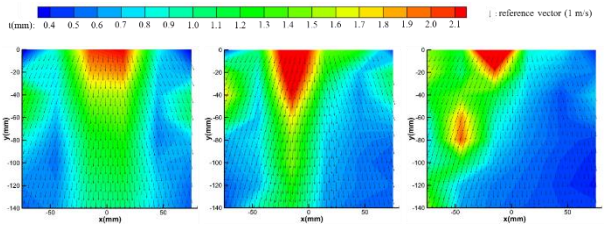

(a) 0 m/s (b) 5 m/s (c) 7 m/s

Fig. 9. Local Liquid Film Velocity and Thickness: Air Velocity Effect

3.4 Uncertainty Analysis

The PIV methods have errors caused by image distortion, the camera set-up condition, the conversion factor, and so on. Therefore, an uncertainty analysis of the volume-PIV method applied to measure the liquid film velocity should be carried out. For the sheet-PIV method, there is a general guide [6] to quantify the error sources. However, the volume-PIV method does not have a generalized guide.

In this paper, a direct comparison experiment between the sheet-PIV and the volume-PIV was carried out. Fig. 10 shows the schematics of the validation experimental facility. The test section was made of acryl with 100 mm × 400 mm × 25 mm (W×H×D) duct geometry. As shown in Figs. 8 (a) and (b), this experimental facility can be adjusted to apply the sheet-PIV and volume-PIV methods. The sheet-PIV method used a laser sheet along the depth direction and a perpendicular view of the high-speed camera. It yielded a velocity profile along the depth, as shown in Fig. 11 (a). At the same positon, the volume-PIV method was also applied. In this case, the high-speed camera took pictures of the test section along the width direction and produced velocity data, as shown in Fig. 11 (b). With the no-slip assumption at the wall, the averaged velocity along the depth direction by the sheet-PIV method was 1.14 m/s. It acted as the total velocity in the uncertainty analysis. The velocity by the volume-PIV method is 1.09 m/s.

The strategy of the uncertainty analysis was as follows. First, we could quantify the expanded error of the sheet-PIV method using a general guide. Second, the difference in the experimental results by the sheet-PIV and the volume-PIV methods corresponds to a bias error in the volume-PIV method. Finally, the expanded error of the volume-PIV with the precision error was quantified.

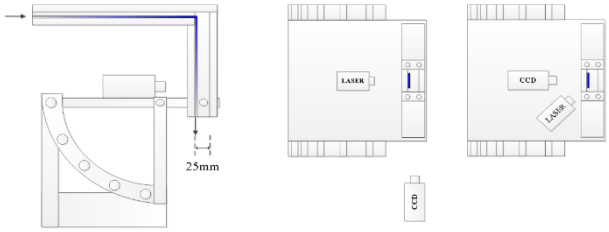

(a) Sheet-PIV (b) Volume-PIV

Fig. 10. Schematics of Validation Experimental Facility

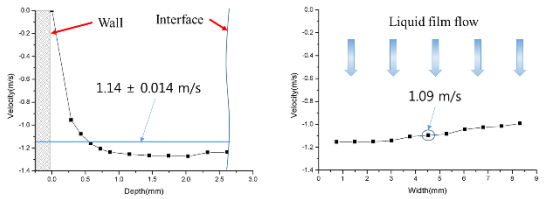

(a) Sheet-PIV (b) Volume-PIV

Fig. 11. Results by Two Different PIV Methods

In this paper, error sources of the sheet-PIV were chosen from it. When the PIV method produces velocity data (u), the error sources come from the magnification factor (α), image displacement (ΔX), time interval (Δt), and experimental error (δu).

$$u=\alpha(\Delta X/\Delta t)+\delta u \qquad (2)$$

The combined error by general guide was about 0.52% (0.00921 m/s). It was applied as a bias error to yield the expanded error of the sheet-PIV method. In addition, the root-sum-square deviations of 11 points of the sheet-PIV results were as follows:

$$\sigma_{RSS} = \sum_{p=1}^{11} \sqrt{B^2 + 2\left(\frac{\bar{\sigma}_p}{\sqrt{n_p}}\right)^2} \qquad (3)$$

where B is the bias error defined by the general guide, $\bar{\sigma}_p$ is the averaged standard deviation of vectors on one position, and n_p is the number of image pairs in the PIV

processing. In Eq. (3), σ_{RSS} was defined by considering the precision error in the range of 95% reliability. Therefore, the expanded error of the sheet-PIV is as shown in Eq. (4):

$$2\bar{\sigma}_1 = \frac{\sigma_{RSS}}{n} = 0.014\ \text{m/s}\ (1.23\%) \qquad (4)$$

The bias error of the volume-PIV can then be defined with the expended error of the sheet-PIV.

$$\text{B} = (\bar{V}_1 + 2\bar{\sigma}_1) - \bar{V}_2 = 0.063\ \text{m/s}\ (5.53\%) \quad (5)$$

where $\bar{V}_1$ and $\bar{V}_2$ were the velocities by the sheet-PIV and volume-PIV, respectively. With the precision error of 500 pairs by the volume-PIV method, the total error can be defined as 5.65%.

Finally, the valid velocity range of the volume-PIV is 1.09 ± 0.06 m/s with 95% reliability. Moreover, the volume-PIV method was valid since the velocity by the sheet-PIV was in the error range.

4. Interfacial Friction Factor Modeling

4.1 Momentum Conservation Equations

To quantify the interfacial friction factor in two-dimensional film flow, interfacial shear stress should be defined by momentum conservation equations. Two-fluid model was suitable to set up the momentum conservation equations for two-dimensional, two-phase flow. Fig. 9 shows the local measurement results and it could be divided into sub-grids to yield the interfacial friction factor as shown in Fig. 12.

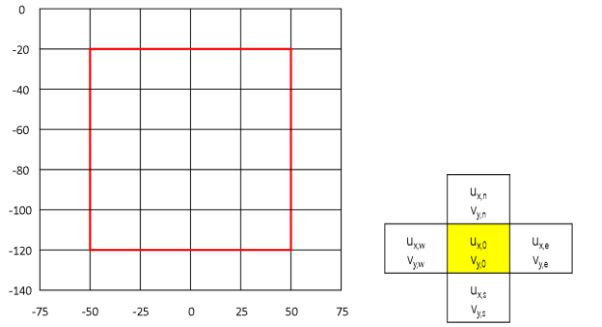

(a) Sub-grids of momentum conservation equations

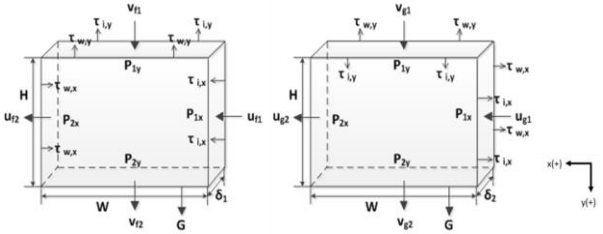

(b) Liquid film (c) Air

Fig. 12. Control Volume Definition for Set-up of Momentum Conservation Equations; film flow in duct can be divided into liquid film flow region and air flow region

A single sub-grid has 25 mm × 20 mm (W×H) length scale, and central sub-grid surrounding with 4 sub-grids produced a local interfacial friction factor. The two-dimensional, two-phase momentum conservation equations could be written as shown in Eqs. (6) ~ (9).

Liquid film

x-direction

$$-(P_2 - P_1)_x \delta_1 H + \int_A \tau_{i,x} dA - \int_A \tau_{wf,x} dA \qquad (6)$$
$$= -\rho_f u_{f\_e} \delta_1 H \left(\frac{u_{f\_e} + u_{f\_0}}{2}\right) + \rho_f u_{f\_0} \delta_1 H \left(\frac{u_{f\_0} + u_{f\_w}}{2}\right)$$
$$-\rho_f u_{f\_n} \delta_1 W \left(\frac{v_{f\_n} + v_{f\_0}}{2}\right) + \rho_f u_{f\_0} \delta_1 W \left(\frac{v_{f\_0} + v_{f\_s}}{2}\right)$$

y-direction

$$-(P_2 - P_1)_y \delta_1 W + \int_A \tau_{i,y} dA - \int_A \tau_{wf,y} dA + \rho_f g \delta_1 H W \qquad (7)$$
$$= -\rho_f v_{f\_n} \delta_1 W \left(\frac{u_{f\_n} + u_{f\_0}}{2}\right) + \rho_f v_{f\_0} \delta_1 W \left(\frac{u_{f\_0} + u_{f\_s}}{2}\right)$$
$$-\rho_f v_{f\_e} \delta_1 H \left(\frac{u_{f\_e} + u_{f\_0}}{2}\right) + \rho_f v_{f\_0} \delta_1 H \left(\frac{u_{f\_0} + u_{f\_w}}{2}\right)$$

Air

x-direction

$$-(P_2 - P_1)_x \delta_2 H + \int_A \tau_{i,x} dA - \int_A \tau_{wg,x} dA \qquad (8)$$
$$= -\rho_g u_{g\_e} \delta_2 H \left(\frac{u_{g\_e} + u_{g\_0}}{2}\right) + \rho_g u_{g\_0} \delta_2 H \left(\frac{u_{g\_0} + u_{g\_w}}{2}\right)$$
$$-\rho_g u_{g\_n} \delta_2 W \left(\frac{v_{g\_n} + v_{g\_0}}{2}\right) + \rho_g u_{g\_0} \delta_2 W \left(\frac{v_{g\_0} + v_{g\_s}}{2}\right)$$

y-direction

$$-(P_2 - P_1)_y \delta_2 W + \int_A \tau_{i,y} dA - \int_A \tau_{wg,y} dA + \rho_g g \delta_2 H W \qquad (9)$$
$$= -\rho_g v_{g\_n} \delta_2 W \left(\frac{u_{g\_n} + u_{g\_0}}{2}\right) + \rho_g v_{g\_0} \delta_2 W \left(\frac{u_{g\_0} + u_{g\_s}}{2}\right)$$
$$-\rho_g v_{g\_e} \delta_2 H \left(\frac{u_{g\_e} + u_{g\_0}}{2}\right) + \rho_g v_{g\_0} \delta_2 H \left(\frac{u_{g\_0} + u_{g\_w}}{2}\right)$$

Pressure differences of each direction could be assumed as same on each phase. Thus, the pressure difference terms of the governing equations can be eliminated. Also assuming uniform air velocity simplified the equations.

x-direction

$$\frac{\int_A \tau_{i,x} dA}{\delta_1 H} - \frac{\int_A \tau_{wf,x} dA}{\delta_1 H} + \frac{\int_A \tau_{i,x} dA}{\delta_2 H} + \frac{\int_A \tau_{wg,x} dA}{\delta_2 H} \qquad (10)$$
$$= -\rho_f u_{f\_e} \left(\frac{u_{f\_e} + u_{f\_0}}{2}\right) + \rho_f u_{f\_0} \left(\frac{u_{f\_0} + u_{f\_w}}{2}\right)$$
$$-\rho_g u_{f\_n} \frac{W}{H} \left(\frac{v_{f\_n} + v_{f\_0}}{2}\right) + \rho_g u_{f\_0} \frac{W}{H} \left(\frac{v_{f\_0} + v_{f\_s}}{2}\right)$$

y-direction

$$-\frac{\int_A \tau_{i,y} dA}{\delta_1 W} - \frac{\int_A \tau_{wf,y} dA}{\delta_1 W} - \frac{\int_A \tau_{i,y} dA}{\delta_2 W} + \rho_f g H - \rho_g g H \qquad (11)$$
$$= -\rho_f v_{f\_n} \left(\frac{v_{f\_n} + v_{f\_0}}{2}\right) + \rho_f v_{f\_0} \left(\frac{v_{f\_0} + v_{f\_s}}{2}\right)$$
$$-\rho_f v_{f\_e} \frac{H}{W} \left(\frac{u_{f\_e} + u_{f\_0}}{2}\right) + \rho_f v_{f\_0} \frac{H}{W} \left(\frac{u_{f\_0} + u_{f\_w}}{2}\right)$$

Interfacial or wall shear stress terms were defined by general descriptions (Eqs. (12) and (13)). The local liquid film velocity and thickness data could not be used to calculate air wall shear stress. Thus Blasius equation was applied to yield wall friction factor of air flow.

$$\int_A \tau_i dA = \int_A \frac{1}{2}\rho_g f_i \left|\overrightarrow{U_g} - \overrightarrow{U_f}\right|\left(U_g - U_f\right)dA \qquad (12)$$

$$\int_A \tau_{wf} dA = \int_A \frac{1}{2}\rho_f f_{wf} U_f \left|\overrightarrow{U_f}\right| dA \qquad (13)$$

4.2 Interfacial Friction Factor

The momentum conservation equations produced local interfacial friction factors. Previous studies [1 ~ 3] mentioned the relation between interfacial friction factor and thickness. In this study, this relation was also confirmed as shown in Fig. 13. The current sets of local data of 5 and 7 m/s lateral air flow indicate that the interfacial friction factor is proportional to the film thickness.

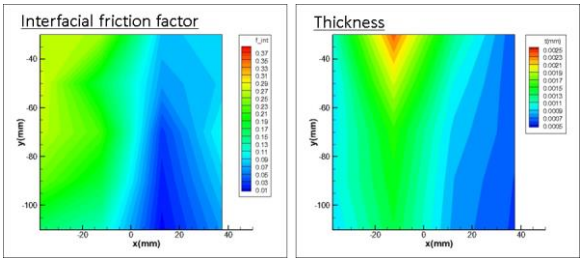

(a) 5m/s

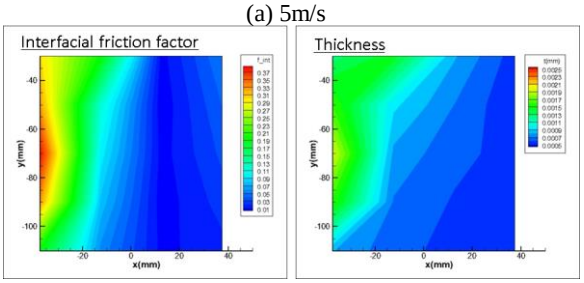

(b) 7m/s

Fig. 13. Relation between interfacial friction factor and film thickness

To compare the interfacial friction factors with previous works, local interfacial friction factors were rearranged by dimensionless film thickness. Hydraulic diameter (D) was duct thickness of test section and film thickness (h) was taken from local measurement data. Fig. 14 shows the comparison results with previous studies. In the case with two-dimensional film flow, the interfacial friction factors are larger than others. The range of dimensionless thickness of the current study is also larger than that of previous studies and the interfacial friction factors are overestimated comparing with previous correlations such as Wallis' model, Fore's model and Asali's data. This result demonstrates that the two-dimensional interfacial drag could be larger than one-dimensional interfacial drag.

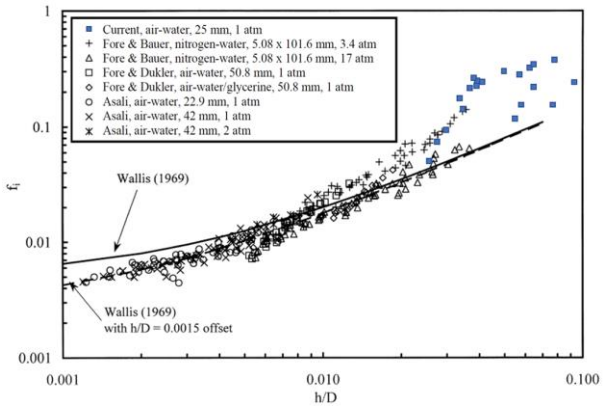

Fig. 14. Comparison of interfacial friction factor with previous studies

3. Conclusions

Two-dimensional two-phase flow on the upper downcomer was simulated with the 1/10 scaled down unfolded test facility. The volume-PIV method was applied to measure the local liquid film velocities. It was validated by general guide of PIV uncertainty analysis and validation experiment. The liquid film thickness data were produced by ultrasonic thickness gauge. The local experimental data were used to calculate the local interfacial friction factor with two-fluid momentum conservation equations. The comparison result with previous interfacial friction models indicates two-dimensional interfacial friction factors are larger than one-dimensional ones.

REFERENCES

[1] G.B. Wallis, "Annular Two-Phase Flow, Part I: Simple Theory," Journal of Fluids Engineering, Vol.92(1), p.59-72 1970.
[2] L.B For, S.G. Beus, R.C. Bauer, "Interfacial friction in gas-liquid annular flow: analogies to full and transition roughness," International Journal of Multiphase Flow, Vol.26, p.1755-1769, 2000.
[3] J. C. Asali, T. J. Hanratty, and P. Andreussi, "Interfacial Drag and Film Height for Vertical Annular Flow," AIChE Journal, Vol.31, No.6, p.895-902, 1985.
[4] B.J. Yun et al. "Scaling for the ECC bypass phenomena during the LBLOCA reflood phase," Nuclear Engineering and Design, Vol.231, p.315-32, 2004.
[5] B. J. Kim et al. "A further assessment of interpolation schemes for window deformation in PIV," Experiments in Fluids, Vol.44, p.499-511, 2006.
[6] S. Nishio et al. "Uncertainty Analysis: Particle Imaging Velocimetry (PIV)," International Towing Tank Conference, Section 7.5-01-03-03, 2008.